
Proceedings Paper:
Mashooq, K and Talukder, MA (2017) Effects of intermediate plasmonic structures on the performance of ultra-thin-film tandem solar cells. In: Proceedings of SPIE - Physics, Simulation, and Photonic Engineering of Photovoltaic Devices VI. SPIE OPTO 2017, 28 Jan - 01 Feb 2017, San Francisco, California, USA. SPIE. Article no: 1009915. ISBN: 9781510606395. ISSN: 0277-786X. EISSN: 1996-756X.

https://doi.org/10.1117/12.2251165

Effects of Intermediate Plasmonic Structures on the Performance of Ultra-Thin-Film Tandem Solar Cells

Kishwar Mashooq and Muhammad Anisuzzaman Talukder*

Department of Electrical and Electronic Engineering

Bangladesh University of Engineering and Technology, Dhaka 1205, Bangladesh

ABSTRACT

Although solar cells can meet the increasing demand for energy of modern world, their usage is not as widespread as expected because of their high production cost and low efficiency. Thin-film and ultra-thin-film solar cells with single and multiple active layers are being investigated to reduce cost. Additionally, multiple active layers of different energy bandgaps are used in tandem in order to absorb the solar spectra more efficiently. However, the efficiency of ultra-thin-film tandem solar cells may suffer significantly mainly because of low photon absorption and current mismatch between active layers. In this work, we study the effects of intermediate plasmonic structures on the performance of ultra-thin-film tandem solar cells. We consider three structures— each with a top amorphous silicon layer and a bottom micro-crystalline silicon layer, and an intermediate plasmonic layer between them. The intermediate layer is either a metal layer with periodic holes or periodic metal strips or periodic metal nano-clusters. Using a finite difference time domain technique for incident AM 1.5 solar spectra, we show that these intermediate layers help to excite different plasmonic and photonic modes for different light polarizations, and thereby, increase the absorption of light significantly. We find that the short-circuit current density increases by ∼12%, ∼6%, and ∼9% when the intermediate plasmonic structure is a metal hole-array, strips, and nano-clusters, respectively, from that of a structure that does not have the intermediate plasmonic layer.

Keywords: Solar cells, Plasmonics, Silicon, Metal layer, Surface plasmons, Extraordinary optical transmission, Light absorption, Short-circuit current density.

1. INTRODUCTION

With the increasing demand for power in modern world, one of the major challenges in our society is to come up with low-cost and environment-friendly energy sources. To address this challenge, significant work has been done on renewable energy sources.[1,2] One of the most promising renewable energy sources is solar cells. Considering the amount of available solar radiation on earth, solar cells have the capability to go a long way to meet the energy needs of today's world.[3] However, because of their high cost and low efficiency, the use of solar cells is not as widespread as one would expect. To address these issues, thin-film and ultra-thin-film solar cells with multiple active layers are being investigated to reduce cost and increase efficiency.[4]

Different nano-photonic techniques are being explored to increase the light absorption in thin-film and ultra-thin-film tandem solar cells so that the cost can be reduced without sacrificing efficiency.[5–10] Two major problems that an ultra-thin-film tandem solar cell face are the very low absorption in ultra-thin active layers and the current mismatch between active layers. Inserting a metal layer between two active layers can effectively eliminate these two problems.[11] An intermediate metal layer facilitates strong coupling of surface modes at the interface of metal and active layer, and thus increases the total absorption in active layers. Additionally, the intermediate metal layer can act as an intermediate electrode, which can effectively eliminate the current mismatch problem.[12]

The intermediate metal layer between two active layers of ultra-thin-film tandem solar cells can be arranged in three fundamental variants— hole-array, strips, and nano-clusters.[11,13,14] Although the total light absorption in active layers increases for all variants of intermediate metal layers, there are significant differences among the optical and electrical properties due to physical arrangements of the intermediate metal layers of these structures.

Muhammad Anisuzzaman Talukder, E-mail: anis@eee.buet.ac.bd

Understanding the opto-electronic behaviors of different intermediate layer arrangements is important to design novel and efficient ultra-thin-film plasmonic tandem solar cells.

In this work, we have compared the optical properties of three different plasmonic ultra-thin-film tandem solar cell structures. As silicon is still the most used material for photovoltaics, we used silicon based tandem solar cells here.[15] We showed that the optical modes can vary significantly with the physical arrangements of intermediate metal layers. Additionally, we found that the strength of the confined Fabry-Perot mode created in plasmonic tandem solar cells strongly depends on the area of the intermediate metal layer. Moreover, we found that the short-circuit current density increases by ∼12%, ∼6%, and ∼9% when the intermediate plasmonic structure is a metal hole-array, strips, and nano-clusters, respectively, from that of a structure that does not have the intermediate plasmonic layer.

The rest of the paper is organized as follows: In Sec. 2, we discuss the structural parameters of plasmonic ultra-thin-film tandem solar cells. In Sec. 3, we discuss the simulation approach of the investigation. In Sec. 4, we discuss the performances of different plasmonic ultra-thin-film tandem solar cells. In Sec. 5, we draw conclusions on the findings.

2. SOLAR CELL STRUCTURES

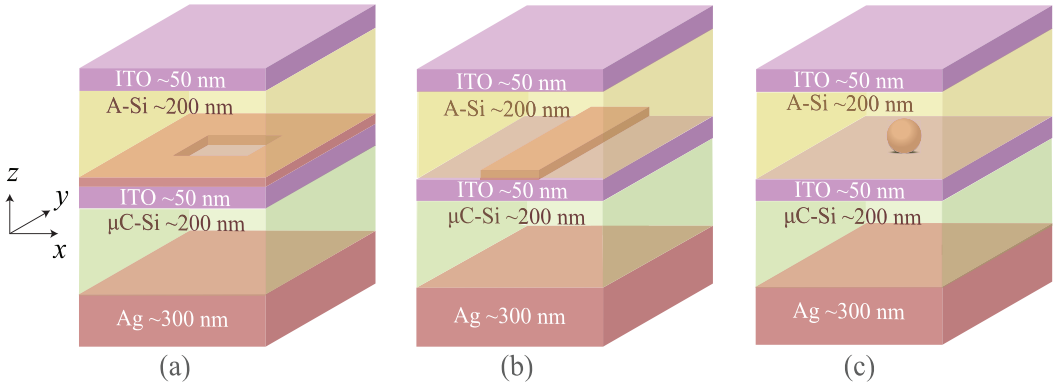

Figure 1. Schematic illustration of ultra-thin-film tandem solar cells with an intermediate metal layer that has (a) hole-array, (b) strips, and (c) nano-clusters.

Schematic illustrations of three variants of ultra-thin-film plasmonic tandem solar cells have been shown in Fig. 1. All the structures are designed to optimize the performance of the structures. Each ultra-thin-film plasmonic tandem solar cell structure has a 200-nm amorphous silicon (A-Si) top and a 200-nm micro-crystalline silicon (μC-Si) bottom active layers. Additionally, a 50-nm ITO layer has been added between the two active layers of all structures, which will facilitate the current conduction through the intermediate electrode. Moreover, another 50-nm ITO layer on the top of A-Si layer, which is used as both current conduction and anti-reflection coating, and a 300-nm silver (Ag) layer at the bottom of μC-Si layer, which is used as the back-contact, have been added.

The plasmonic tandem solar cell structure in Fig. 1(a) has an intermediate metallic hole-array layer with a thickness of 20 nm and a square hole width of 40 nm. The structure in Fig. 1(b) has an intermediate metallic strip with height of 20 nm and width of 20 nm. The structure in Fig. 1(c) has an intermediate metallic nano-cluster with cluster radius of 10 nm. The periodicity of the unit solar cells of the structures in Figs. 1(a), 1(b), and 1(c) are 80 nm, 80 nm, and 50 nm, respectively.

3. SIMULATION APPROACH

To calculate the absorption of solar spectra in the active regions of different structures, we have solved Maxwell's equations using full-field finite difference time domain (FDTD) method. For simulation, we considered a broad-band plane wave source of 400–1300 nm range. To minimize diffraction effects, the light source has been placed

at a sufficient height from the top surface. Since the structures shown in Fig. 1 are periodic in both the x- and y-directions, we consider only one period of the structures and apply periodic boundary conditions in both the x- and y-directions. By contrast, we apply a perfectly matched layer boundary condition in the z-direction. In simulation, we used grid sizes that are much smaller than the feature sizes so that an insufficient density of mesh grids does not induce divergent electromagnetic field distribution, and hence inaccurate results. We have checked the accuracy and convergence of results by increasing the number of grid points twice at each step until there is no noticeable change in the results. The power absorption per wavelength is calculated by using the equation

$$P_{\text{abs}} = -\frac{1}{2}\int_v \omega|\vec{E}|^2 \text{Im}(\epsilon) dv, \tag{1}$$

where $\vec{E}$ is the steady state electric field, ω is the angular frequency and ϵ is the permittivity of the material. The total absorption is calculated for both TE- and TM-incident light and normalized for broadband plane wave source. We have also calculated the short-circuit current density for AM 1.5 solar spectra assuming that each absorbed photon creates an EHP and all photo-generated EHPs are collected at the terminals.

4. PERFORMANCE ANALYSIS

The intermediate metal layers between two sub-cells of the structures in Fig. 1 scatter the incident light and help to couple surface modes at the interface of metal-active layers region. As the light-matter interaction of a region is determined by the magnitude of local electric field, creating surface modes at the interface of metal-active layer region significantly increases the total absorption, and hence the short-circuit current density in the sub-cells. In this work, we have only considered normal incidence of solar spectra on the structures. As the surface modes created inside the structures will highly depend on the polarization of incident light, we have considered both TM- and TE-polarized incident light. Since the solar spectra are unpolarized, we have considered a combination of 50% TM-polarized light and 50% TE-polarized light to calculate the short-circuit current densities of the structures.

4.1 Solar cell structure with intermediate hole-array layer

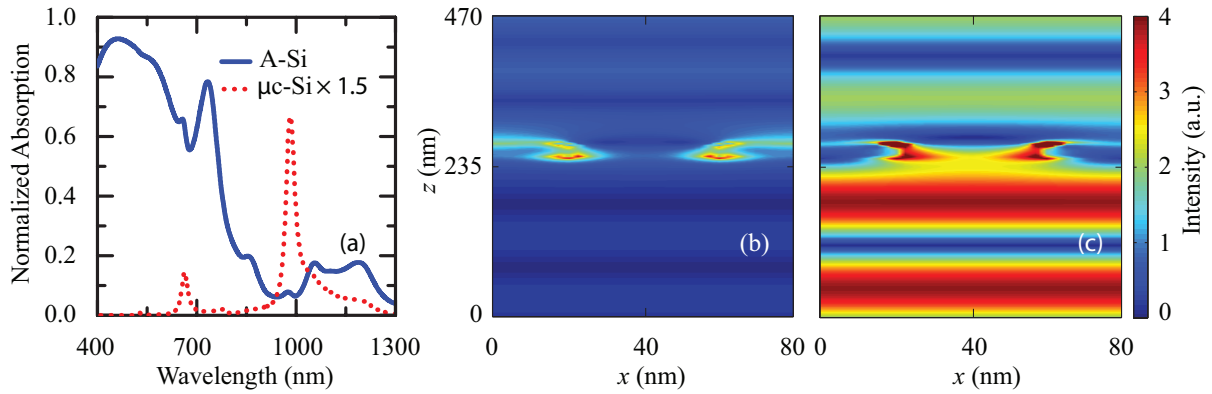

Figure 2. (a) Normalized absorption spectra for TM-polarized normal incident light in A-Si and μc-Si sub-cells for the structure in Fig. 1(a). Electric field intensity in x-z plane at $y = 0$ for incident TM-polarized light in the structure with an intermediate metallic hole-array layer at wavelengths of (b) 655 nm and (c) 970 nm.

The structure with intermediate metallic hole-array that is shown in Fig. 1(a), funnels majority portion of light through the holes in metallic hole array and helps to couple surface plasmons (SPs) at the interface of metal-active layer region and highly localized cut-off resonance.[16] This phenomenon is commonly known as extraordinary optical transmission. By coupling these modes, the periodic metallic hole-array significantly improves the performance of the ultra-thin film tandem solar cell. Additionally, the presence of intermediate metallic hole-array layer forms a strong Fabry-Perot resonance with the bottom back-contact and relatively weak Fabry-Perot resonance with the top ITO layer, which are not created for traditional tandem solar cells.

In Fig. 2(a), we show the normalized absorption of incident light into the top A-Si and bottom μC-Si sub-cells for TM-polarized normal incident light. As the structure is symmetric, the light absorption in both sub-cells, and hence the short-circuit current density remains the same for both normal TM- and TE-polarized light. In Figs. 2(b) and 2(c), we present two-dimensional electric field intensity in the x-z planes at wavelengths of 655 nm and 970 nm, respectively. In Fig. 2(b), we note that the incident light mainly couples to SPs at 655 nm. However, The strong excitation of localized cut-off resonance and Fabry-Perot resonance at 970 nm is clear in Fig. 2(c), where we plot the normalized electric field profile intensity in the x-z plane through the center of the hole. As the intermediate metallic layer covers ∼75% area of the unit solar cell, the coupling of Fabry-Perot resonance is very strong at wavelength of 970 nm. These strong modes significantly increase the total short-circuit current density in both sub-cells. The short-circuit current densities in the top A-Si sub-cell and bottom μC-Si sub-cell are ∼203 Am^{-2} and ∼12 Am^{-2}, respectively. The total short-circuit current density is ∼12% greater than that in a tandem cell without the intermediate hole-array layer.

4.2 Solar cell structure with intermediate strip layer

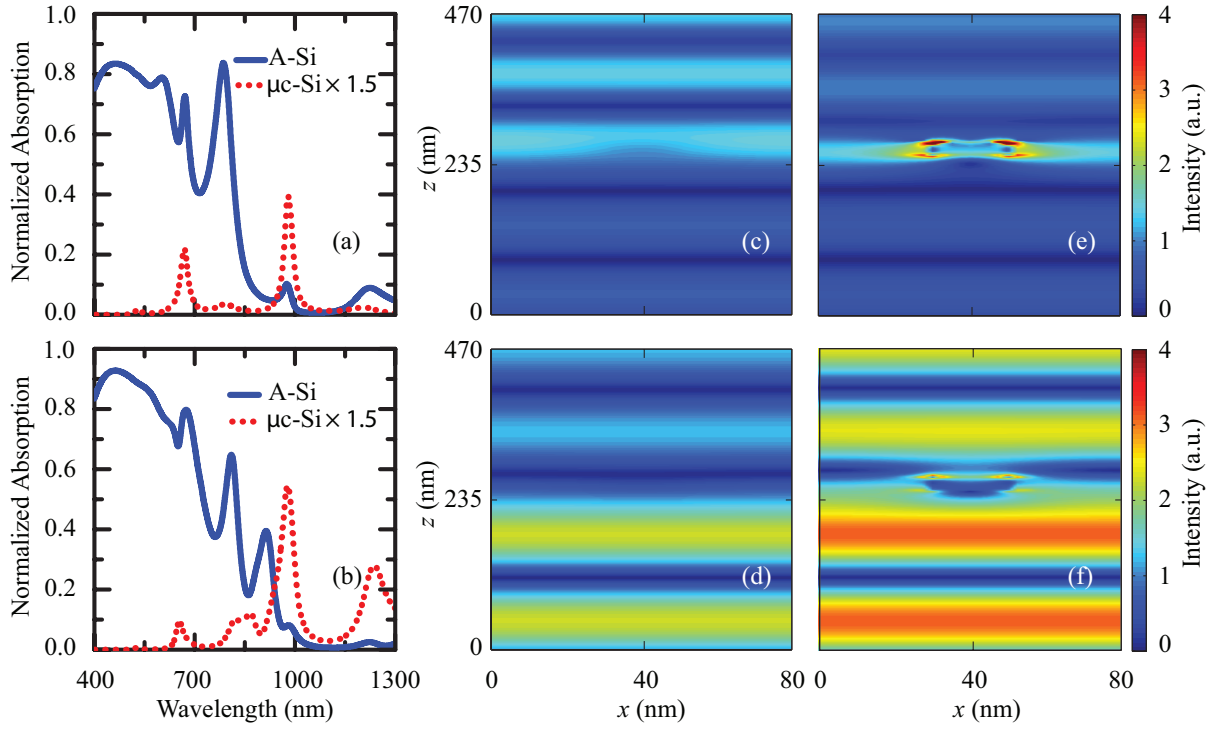

Figure 3. Normalized absorption spectra in A-Si and μc-Si sub-cells for the structure in Fig. 1(b) for (a) TE-polarized normal incident light and (b) TM-polarized normal incident light. Electric field intensity in x-z plane at $y = 0$ for incident TE-polarized light in the structure with an intermediate metallic strip layer at wavelengths of (c) 655 nm and (d) 970 nm. Electric field intensity in x-z plane at $y = 0$ for incident TM-polarized light in the structure with an intermediate metallic strip layer at wavelengths of (e) 835 nm and (f) 970 nm.

In the structure with metallic strip that is shown in Fig. 1(b), the metallic strip helps the incident light to couple to surface plasmons when the light is incident normally and TM-polarized. Due to the asymmetry of the structure, SP mode cannot be coupled at metal-active region interface when the light is incident normally and TE-polarized. Therefore, in case of normally incident TE-polarized light, the absorption is enhanced by photonic modes created by the scattering of light, which is enhanced by the metallic strip between the sub-cells.[17] However, the polarization-dependent absorption severely damages the overall performance of this solar cell.

In Figs. 3(a) and 3(b), we show the normalized absorption of incident light into the top A-Si and bottom μC-

Si sub-cells for TE- and TM-polarized normal incident light, respectively. We note that the absorption in both top and bottom sub-cells significantly decreases when the polarization of light changes from TM-polarization to TE-polarization. In Figs. 3(c) and 3(d), we present two-dimensional electric field intensity in the x-z planes at wavelengths of 655 nm and 970 nm for TE-polarized light, respectively. In both cases, we note that the incident light mainly couples to weak Fabry-Perot modes as the normal TE-polarized light does not facilitate any surface modes for this structure. In Figs. 3(e) and 3(f), we present two-dimensional electric field intensity in the x-z planes at wavelengths of 835 nm and 970 nm for TM-polarized light, respectively. We note the strong excitation of a surface plasmon mode at 835 nm in Fig. 3(e). Figure 3(f) shows the Fabry-Perot resonance is created inside both top and bottom sub-cells, which will not be present without the intermediate layer. However, as the intermediate metallic layer covers ∼25% area of the unit solar cell, the coupling of Fabry-Perot resonance is relatively weaker at wavelength of 970 nm than that of the structure of Fig. 1(a). The short-circuit current densities are ∼195 Am^{-2} and ∼9 Am^{-2} in A-Si and μc-Si layers, respectively, and the total short-circuit current density is ∼6% greater than that in a tandem cell without intermediate metallic strip layer.

4.3 Solar cell structure with intermediate nano-cluster layer

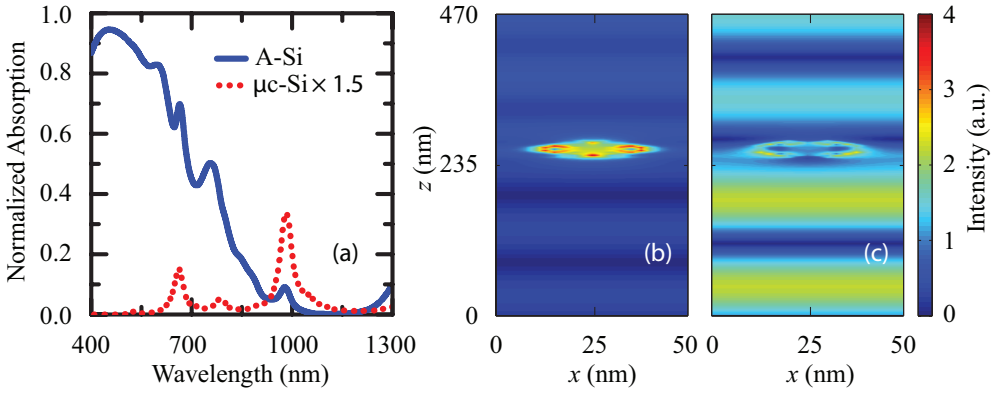

Figure 4. (a) Normalized absorption spectra for TM-polarized light in top A-Si and bottom μc-Si sub-cells for the structure in Fig. 1(c). Electric field intensity in x-z plane at $y = 0$ for incident TM-polarized light in the structure with an intermediate metallic nanocluster layer at wavelengths of (b) 645 nm and (c) 970 nm.

In the structure with metallic nanoclusters that is shown in Fig. 1(c), the metallic nano-clusters help the incident light to couple to localized surface plamons (LSPs), and thus, enhance the total light absorption in the structure. In Fig. 4(a), we show the normalized absorption of incident light into the top A-Si and bottom μC-Si sub-cells for TM-polarized normal incident light. As the structure is symmetric, the light absorption in both sub-cells, and hence the short-circuit current density remains the same for both normal TM- and TE-polarized light. In Figs. 4(b) and 4(c), we present two-dimensional electric field intensity in the x-z planes at wavelengths of 645 nm and 970 nm, respectively. In Fig. 4(b), we note that the incident light mainly couples to strong LSPs at 645 nm, which mainly increases the absorption in top sub-cell. Additionally, in Fig. 4(c), we note a Fabry-Perot resonance in both layers. As the intermediate metallic nanocluster layer covers ∼5% area of the unit solar cell, the coupling of Fabry-Perot resonance is weaker at wavelength of 970 nm than that of the structure in Figs. 1(a) and 1(b). The short-circuit current densities in the top A-Si sub-cell and bottom μC-Si sub-cell are ∼202 Am^{-2} and ∼6 Am^{-2}, respectively. The total short-circuit current density is ∼12% greater than that in a tandem cell without the intermediate hole-array layer.

5. CONCLUSION

In this work, we have investigated the role of intermediate metal layer in plasmonic ultra-thin-film tandem solar cells. The excitation mechanism varies with different physical arrangements of intermediate metal layer. We have identified three major modes working in plasmonic tandem solar cells– surface plasmon modes, localized cut-off resonance, and confined Fabry-Perot resonance. Depending on the polarization of light and arrangement

of intermediate metal layer, the generation and coupling of these modes vary greatly. Additionally, we found that the strength of the confined Fabry-Perot mode in plasmonic solar cells depends on the area of the intermediate metal layer. Because of different modes, the total light absorption and the short-circuit current density change with the arrangement of intermediate metal layer. However, in all cases, the short-circuit current density increases with respect to similar traditional tandem solar cell. We note that the short-circuit current density increases by ∼12%, ∼6%, and ∼9% when the intermediate plasmonic structure is a metal hole-array, strips, and nano-clusters, respectively, from that of a structure that does not have the intermediate plasmonic layer. This work explores the underlying optical properties of plasmonic tandem solar cells with different intermediate metal layers and will serve as a guideline to create next generation plasmonic tandem solar cells.

REFERENCES

[1] Dincer, I., "Renewable energy and sustainable development: a crucial review," Renew. Sust. Energ. Rev. **4**(2), 157–175 (2000).

[2] Hossain, M. M. and Ali, M. H., "Future research directions for the wind turbine generator system," Renew. Sust. Energ. Rev. **49**, 481–489 (2015).

[3] Lewis, N. S., "Powering the Planet," MRS Bull. **32**(10), 808–820 (2007).

[4] Li, G., Li, H., Ho, J. Y. L. , Wong, M. and Kwok, H. S., "Nanopyramid Structure for Ultrathin c-Si Tandem Solar Cells," Nano Lett. **14**(5), 2563–2568 (2014).

[5] Atwater, H. A. and Polman, A., "Plasmonics for improved photovoltaic devices," Nat. Mater. **9**(10), 205–213 (2010).

[6] Zhu, J., Hsu, C. M., Yu, Z., Fan, S. and Cui, Y., "Nanodome Solar Cells with Efficient Light Management and Self-Cleaning," Nano Lett. **10**(6), 1979–1984 (2010).

[7] Naughton, M. J., Kempa, K., Ren, Z. F., Gao, Y., Rybczynski, J., Argenti, N., Gao, W., Wang, Y., Peng, Y., Naughton, J. R., McMahon, G., Paudel, T., Lan, Y. C., Burns, M. J., Shepard, A., Clary, M., Ballif, C., Haug, F. J., Soederstroem, T., Cubero, O. and Eminian, C., "Efficient nanocoax-based solar cells," Phys. Status Solidi RRL **4**(7), 181–183 (2010).

[8] Biswas, R., Bhattacharya, J., Lewis, B., Chakravarty, N. and Dalal, V., "Enhanced nanocrystalline silicon solar cell with a photonic crystal back-reflector," Sol. Energy Mater. Sol. Cells **94**(12), 2337–2342 (2010).

[9] Mallick, S. B., Agrawal, M., and Peumans, P., "Optimal light trapping in ultra-thin photonic crystal crystalline silicon solar cells," Opt. Express **18**(6), 5691–5706 (2010).

[10] Awal, M. A., Ahmed, Z. and Talukder, M. A., "An efficient plasmonic photovoltaic structure using silicon strip-loaded geometry," J. Appl. Phys. **117**(6), 063109 (2015).

[11] Mashooq, K. and Talukder, M. A., "Management of light absorption in extraordinary optical transmission based ultra-thin-film tandem solar cells," J. Appl. Phys. **119**(19), 193101 (2016).

[12] Zhang, X., Huang, Q., Hu, J., Knize, R. J. and Lu, Y., "Hybrid tandem solar cell enhanced by a metallic hole-array as the intermediate electrode," Opt. Express **22**(6), A1400–A1411 (2014).

[13] Rachi, M. R. K., Jawad, N. and Talukder, M. A., "Enhancement of light absorption in a thin-film tandem solar cell with an intermediate layer of metal strips," IEEE Photonics Conference (IPC), Virginia, USA (2015).

[14] Wang, W., Wu, S., Reinhardt, K., Lu, Y. and Chen, S., "Broadband Light Absorption Enhancement in Thin-Film Silicon Solar Cells," Nano Lett. **10**(6), 2012-18 (2010).

[15] Saga, T., "Advances in crystalline silicon solar cell technology for industrial mass production," NPG Asia Mater. **2**(3), 96–102 (2010).

[16] Rodrigo, S. G., [Optical properties of Nanostructured metallic system studied with Finite Difference Time-Domain method], Springer, Berlin & Heidelberg, 37—73 (2012).

[17] Mokkapati, S., Beck, F. J., Waele, R. de, Polman, A. and Catchpole, K. R., " Resonant nano-antennas for light trapping plasmonic solar cells," J. Phys. D: Appl. Phys. **44**, 185101 (2011).